

Physics-based modelling for a closed form solution for flow angle estimation

Angelo Lerro*¹

¹Department of Mechanical and Aerospace Engineering, Polytechnic University of Turin, C.so Duca degli Abruzzi
24 Turin, 10129, Italy

(Received June 21, 2021, Revised July 26, 2021, Accepted November 30, 2021)

Abstract. Model-based, data-driven and physics-based approaches represent the state-of-the-art techniques to estimate the aircraft flow angles, angle-of-attack and angle-of-sideslip, in avionics. Thanks to sensor fusion techniques, a synthetic sensor is able to provide estimation of flow angles without any dedicated physical sensors. The work deals with a physics-based scheme derived from flight mechanic theory that leads to a nonlinear flow angle model. Even though several solvers can be adopted, nonlinear models can be replaced with less accurate but straightforward ones in practical applications. The present work proposes a linearisation to obtain the flow angles' closed form solution that is verified using a flight simulator. The main objective of the paper, in fact, is to analyse the estimation degradation using the proposed closed form solutions with respect to the nonlinear scheme. Moreover, flight conditions, where the proposed closed form solutions are not applicable, are identified.

Keywords: flow angles; flight mechanics; model-free

1. Introduction

State-of-the-art flow angle sensors are typically probes and vanes protruding externally from the aircraft fuselage able to provide a direct measure of air data, mainly pressures (Gavrilovic *et al.* 2018) or flow angles (Popowski and Dabrowski 2015). A synthetic sensor is basically a method able to provide flow angle estimations by means of fusing together flight data already available on board from other systems, e.g. the inertial reference system.

In the era of digital avionics, synthetic sensors can be added to physical (or mechanical) sensors in order to analytically increase the system redundancy (Fravolini *et al.* 2019, Marzat *et al.* 2012). Another possible application is to use synthetic sensors to monitor physical sensors and to accommodate possible failures (Pouliezios and Stavrakakis 1994). Moreover, the concurrent use of dissimilar sources of the same air data (physical and synthetic ones) can be beneficial to solve some issues related to common failure modes or incorrect failure diagnosis of modern air data system (Eubank *et al.* 2010, Lu *et al.* 2020).

*Corresponding author, Angelo Lerro, Ph.D., E-mail: angelo.lerro@polito.it

A very first example of synthetic estimation of flow angles can be found in (Dendy and Transier 1969, Freeman 1973), model-based (e.g. Kalman filter in (Tian *et al.* 2021)) and data-driven (e.g. neural networks in (Colgren *et al.* 1999)) are the approaches commonly used to estimate flow angles that are designed ad hoc for a particular aircraft. The latter aspect limits the use of synthetic sensors to a specific aircraft configuration and a flight regime. A physics-based, or model-free, nonlinear scheme, named ASSE, was proposed (Lerro *et al.* 2021) aiming to be independent by the aircraft application. The nonlinear ASSE scheme requires specific solver, such as iterative methods. Nevertheless, some practical considerations (e.g. about computing and certification efforts) could limit the use of nonlinear schemes in favour of less accurate but straightforward approaches.

In order to avoid to use iterative methods for flow angles estimations, the present work introduces the linearisation of the ASSE scheme to define a flow angle's closed form solution that is model-free, i.e. not dependent on the specific aircraft application. The main objectives of the paper, in fact, are to 1) evaluate the closed form solution's existence conditions, 2) analyse closed form solution performance degradation with respect to the nonlinear ASSE scheme and 3) identify flight conditions where the proposed linearisation is not applicable.

Notations used in this work are described in section 2. After a brief introduction of the nonlinear ASSE scheme, the proposed linear ASSE scheme and the closed form solutions for flow angles are presented in section 3. Proposed linear solutions' existence conditions are emphasised in section 4 and accuracy limitations in section 5. Numerical results and error analysis are discussed in section 6 highlighting flight conditions where the linear ASSE scheme is not reliable.

2. Notations

In this work, two reference frames are considered: the inertial reference frame $\mathcal{F}_I = \{X_I, Y_I, Z_I\}$ and the body reference frame $\mathcal{F}_B = \{X_B, Y_B, Z_B\}$ as described in the Fig. 1. The vector subscript denotes the reference frame where the vector is represented.

The typical velocity triangle (Nelson 1989) made up of the inertial velocity \mathbf{v}_I , the relative velocity \mathbf{v}_B and the wind velocity \mathbf{w}_I can be written as

$$\mathbf{v}_I = \mathbf{C}_{B2I}\mathbf{v}_B + \mathbf{w}_I \quad (1)$$

where \mathbf{C}_{B2I} is the direction-cosine matrix to calculate vector components in the inertial reference frame from the body reference frame (Schmidt 2011). Considering the time derivative properties (Salychev 2004), Eq. (1) can be derived to find the expression of the coordinate acceleration vector $\mathbf{a}_I = \dot{\mathbf{v}}_I$ and its representation in the body reference frame as

$$\mathbf{a}_B = \mathbf{C}_{I2B}\mathbf{a}_I = \dot{\mathbf{v}}_B + \boldsymbol{\Omega}_B\mathbf{v}_B + \mathbf{C}_{I2B}\dot{\mathbf{w}}_I = a_{X_B}\hat{\mathbf{i}}_B + a_{Y_B}\hat{\mathbf{j}}_B + a_{Z_B}\hat{\mathbf{k}}_B \quad (2)$$

where $\boldsymbol{\Omega}_B$ is defined as the body angular rate matrix (Etkin and Reid 1995) and $\hat{\mathbf{i}}_B$, $\hat{\mathbf{j}}_B$ and $\hat{\mathbf{k}}_B$ are three unit vectors defining the body reference axes. The time derivative of the wind vector in the body reference frame can be expressed as $\mathbf{C}_{I2B}\dot{\mathbf{w}}_I = (\mathbf{C}_{I2B}\dot{\mathbf{w}}_I)_{X_B}\hat{\mathbf{i}}_B + (\mathbf{C}_{I2B}\dot{\mathbf{w}}_I)_{Y_B}\hat{\mathbf{j}}_B + (\mathbf{C}_{I2B}\dot{\mathbf{w}}_I)_{Z_B}\hat{\mathbf{k}}_B$. It is worth highlighting that the coordinate acceleration

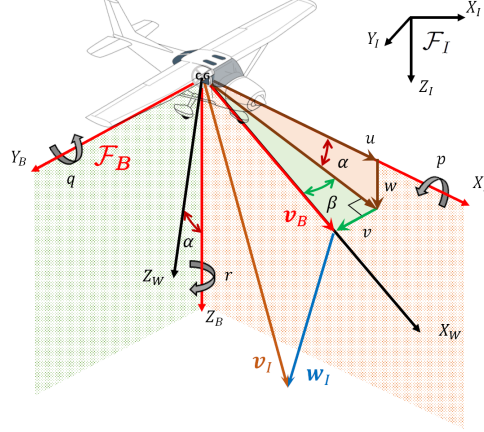


Fig. 1 Representation of inertial and body reference frames with positive flow angles (α , β), linear relative velocities (u , v , w), angular rates (p , q , r) and the velocity triangle between inertial velocity \mathbf{v}_I , the relative velocity \mathbf{v}_B and the wind velocity \mathbf{w}_I .

can be calculated from the inertial acceleration usually measured on board by inertial reference systems when the Euler angles are known.

The relative velocity \mathbf{v}_B can be expressed as function of its module and flow angles as

$$\mathbf{v}_B = V_\infty \hat{\mathbf{i}}_{WB} = (\cos \beta \cos \alpha) \hat{\mathbf{i}}_B + (\sin \beta) \hat{\mathbf{j}}_B + (\cos \beta \sin \alpha) \hat{\mathbf{k}}_B \quad (3)$$

where V_∞ is the magnitude of the relative velocity vector, $V_\infty = |\mathbf{v}_B| = \sqrt{u^2 + v^2 + w^2}$, $\hat{\mathbf{i}}_{WB}$ is the versor of \mathbf{v}_B .

3. Proposed Linearisation

3.1 Nonlinear Scheme Synopsis

According to the ASSE scheme introduced in (Lerro *et al.* 2021), the time-derivative of the relative velocity's magnitude can be expressed as

$$\dot{V}_\infty V_\infty = \mathbf{v}_B^T \dot{\mathbf{v}}_B = \mathbf{v}_B^T (\mathbf{a}_B - \mathbf{C}_{I2B} \dot{\mathbf{w}}_I) \quad (4)$$

where all terms are measured at the same time instant. Moreover, the relative velocity vector \mathbf{v}_B at time t can be expressed starting from \mathbf{v}_B at a generic time τ , with $t \geq \tau$, as

$$\mathbf{v}_B(t) = \mathbf{v}_B(\tau) + \int_\tau^t \dot{\mathbf{v}}_B(\mathcal{T}) d\mathcal{T} \quad (5)$$

Henceforth, in order to ease the notation, the independent variable of the integrand function is omitted and the time of the measure is reported as subscript. For example, the relative velocity evaluated at time τ is denoted as $\mathbf{v}_{B,\tau}$.

Recalling Eq. (2), Eq. (5) can be rewritten as

$$\mathbf{v}_{B,t} = \mathbf{v}_{B,\tau} + \int_{\tau}^t (\mathbf{a}_B - \boldsymbol{\Omega}_B \mathbf{v}_B - \mathbf{C}_{I2B} \dot{\mathbf{w}}_I) d\mathcal{T} \quad (6)$$

and

$$\mathbf{v}_{B,\tau} = \mathbf{v}_{B,t} - \int_{\tau}^t \mathbf{a}_B d\mathcal{T} + \int_{\tau}^t \boldsymbol{\Omega}_B \mathbf{v}_B d\mathcal{T} + \int_{\tau}^t \mathbf{C}_{I2B} \dot{\mathbf{w}}_I d\mathcal{T} \quad (7)$$

Replacing $\mathbf{v}_{B,\tau}$ with Eq. (7), Eq. (4) can be written at time τ as

$$V_{\infty,\tau} \dot{V}_{\infty,\tau} = \left[\mathbf{v}_{B,t} + \int_{\tau}^t \boldsymbol{\Omega}_B \mathbf{v}_B d\mathcal{T} \right]^T (\mathbf{a}_B - \mathbf{C}_{I2B} \dot{\mathbf{w}}_I)_{\tau} \quad (8)$$

where all terms depending on \mathbf{v}_B , and hence on the flow angles, are collected on the right hand side.

The ASSE scheme based on the zero-order approximation (Lerro *et al.* 2021) assumes that the integral term $\int_{\tau}^t \boldsymbol{\Omega}_B \mathbf{v}_B d\mathcal{T}$ of Eq. (8) is constant in the generic time interval $[\tau, t]$, therefore

$$\int_{\tau}^t \boldsymbol{\Omega}_B \mathbf{v}_B d\mathcal{T} = (\boldsymbol{\Omega}_B \mathbf{v}_B)_t \Delta t, \quad (9)$$

where $\Delta t = t - \tau$. Considering the latter expression, Eq. (8) can be rewritten as

$$\begin{aligned} V_{\infty,\tau} \dot{V}_{\infty,\tau} + \left[\int_{\tau}^t \mathbf{a}_B d\mathcal{T} - \int_{\tau}^t \mathbf{C}_{I2B} \dot{\mathbf{w}}_I d\mathcal{T} \right]^T (\mathbf{a}_B - \dot{\mathbf{w}}_B \mathbf{C}_{I2B} \dot{\mathbf{w}}_I)_{\tau} = \\ = V_{\infty,t} \hat{\mathbf{i}}_{WB,t}^T (\mathbf{I} - \boldsymbol{\Omega}_{B,t} \Delta t) (\mathbf{a}_B - \mathbf{C}_{I2B} \dot{\mathbf{w}}_I)_{\tau} \end{aligned} \quad (10)$$

Eq. (10) is denoted in (Lerro *et al.* 2021) as the basic expression of the zero-order ASSE scheme referred to the generic time τ where the flow angles, $\alpha(t)$ and $\beta(t)$, are the only unknowns and all other terms are supposed to be measured. For the latter reason, the unknown variables are always referred to current time t , henceforth, the flow angles are represented without subscripts related to time.

3.2 Closed Form Solution

Considering Taylor series expansions of trigonometric functions, the versor of Eq. (3) can be approximated at first order (i.e. $\cos(x) \approx 1$ and $\sin(x) \approx x$) as:

$$\hat{\mathbf{i}}_{WB,t} \approx \tilde{\mathbf{i}}_{WB,t} = [1, \beta, \alpha]^T \quad (11)$$

The proposed approximation is valid, for example, when AoA and AoS are $< 15^\circ$ as absolute values. Even though the latter hypothesis limits the use of the proposed solution, it is still applicable in the most of the aircraft operative flight envelope. As the unknown variables are two flow angles at time t , the proposed linearised scheme is based on two equations. Therefore, writing Eq. (10) for time t and a generic previous time τ (with $\tau < t$), the following system of two linear equations is obtained

$$\begin{cases} \tilde{\mathbf{i}}_{WB,t}^T (\mathbf{a}_B - \mathbf{C}_{I2B} \dot{\mathbf{w}}_I)_t = \dot{V}_{\infty,t} \\ V_{\infty,t} \tilde{\mathbf{i}}_{WB,t}^T (\mathbf{I} - \boldsymbol{\Omega}_{B,t} \Delta t) (\mathbf{a}_B - \mathbf{C}_{I2B} \dot{\mathbf{w}}_I)_\tau = \\ = V_{\infty,\tau} \dot{V}_{\infty,\tau} + \left[\int_\tau^t \mathbf{a}_B d\mathcal{T} - \int_\tau^t \mathbf{C}_{I2B} \dot{\mathbf{w}}_I d\mathcal{T} \right]^T (\mathbf{a}_B - \mathbf{C}_{I2B} \dot{\mathbf{w}}_I)_\tau \end{cases} \quad (12)$$

In order to simplify the proposed scheme notations, the measurable quantities of Eq. (10) are grouped and denoted as follows

$$n_\tau = V_{\infty,\tau} \dot{V}_{\infty,\tau} + \left[\int_\tau^t \mathbf{a}_B d\mathcal{T} - \int_\tau^t \mathbf{C}_{I2B} \dot{\mathbf{w}}_I d\mathcal{T} \right]^T (\mathbf{a}_B - \mathbf{C}_{I2B} \dot{\mathbf{w}}_I)_\tau \quad (13)$$

and

$$\mathbf{m}_\tau = V_{\infty,t} (\mathbf{I} - \boldsymbol{\Omega}_{B,t} \Delta t) (\mathbf{a}_B - \mathbf{C}_{I2B} \dot{\mathbf{w}}_I)_\tau = h_\tau \hat{\mathbf{i}}_B + l_\tau \hat{\mathbf{j}}_B + m_\tau \hat{\mathbf{k}}_B \quad (14)$$

Therefore, the linear system of Eq. (12) can be rewritten in a more compact form

$$\begin{cases} n_t = \hat{\mathbf{i}}_{WB,t}^T \mathbf{m}_t \approx h_t + l_t \beta_{lin} + m_t \alpha_{lin} \\ n_\tau = \hat{\mathbf{i}}_{WB,t}^T \mathbf{m}_\tau \approx \tilde{\mathbf{i}}_{WB,t}^T \mathbf{m}_\tau = h_\tau + l_\tau \beta_{lin} + m_\tau \alpha_{lin} \end{cases} \quad (15)$$

It is worth highlighting that the system of Eq. (12) is based on a previous time τ , but, for the sake of generality, the same generic τ can be also consecutive to current time t . Using the Cramer's rule to solve the system of Eq. (15), the closed form solutions for flow angle are obtained as

$$\begin{cases} \alpha_{lin} = \frac{l_t(n_\tau - h_\tau) - l_\tau(n_t - h_t)}{D} \\ \beta_{lin} = \frac{m_\tau(n_t - h_t) - m_t(n_\tau - h_\tau)}{D} \end{cases} \quad (16)$$

where $D = l_t m_\tau - m_t l_\tau$ is the determinant of the system. Therefore, the proposed linear estimation of flow angles is based on direct measures of: 1) true airspeed, V_∞ , and its time derivative, \dot{V}_∞ ; 2) the coordinate body acceleration \mathbf{a}_B ; 3) angular rates; 4) the wind acceleration.

4. Existence Conditions

The proposed linearised ASSE scheme has a unique couple of solutions for α and β only when the determinant D is nonzero. The first existence condition equation can be written as

$$D = l_t m_{\tau_1} - m_t l_{\tau_1} \neq 0 \quad (17)$$

As found in (Lerro *et al.* 2021), two equations is the minimum number to be considered and the two corresponding time steps shall introduce two independent equations in order to guarantee that the determinant D is nonzero, or conversely that the system of Eq. (15) has

linearly independent rows. Moreover, both equations cannot be referred to trim conditions otherwise it would lead to a null determinant. In fact, as also observed in (Sun *et al.* 2018), the analytical flow angle estimation (based on a model-free approach) cannot be performed in uniform flight (or trim) conditions.

It is worth highlighting that D can be evaluated a priori to verify that the first existence condition of solutions for AoA and AoS (i.e. not uniform flight conditions and two independent equations) is satisfied.

5. Limitations of the Proposed Closed Form Solutions

The same results of Eq. (16) can be achieved using the substituting method that is useful to highlight a more explicit relationship between α_{lin} and β_{lin} . Solving the first equation of Eq. (15) as function of one flow angle, we can rewrite the proposed closed form solutions in the following form:

$$\begin{aligned}\alpha_{lin} &= \frac{n_t - h_t - l_t \beta_{lin}}{m_t} \\ \beta_{lin} &= \frac{n_t - h_t - m_t \alpha_{lin}}{l_t}\end{aligned}\tag{18}$$

From Eq. (18), it is clear that the proposed linearisation leads to undefined solution for AoA when m_t tends to zero, for AoS when l_t tends to zero. Therefore, additional existence conditions are

$$\begin{aligned}m_t &\neq 0 \\ l_t &\neq 0\end{aligned}\tag{19}$$

5.1 Negligible Wind Acceleration

If the wind is constant or null, the proposed scheme is only affected by errors introduced with the 0-order approximation (Lerro *et al.* 2021) and the small angle hypothesis.

Generally speaking, the proposed closed form solution is based on the hypothesis that the wind acceleration vector $\dot{\mathbf{w}}$ is known, i.e. measured, or it is negligible. The first hypothesis is obviously not practical, whereas the second hypothesis can be applicable in some circumstances. In fact, considering that the linearisation of the flow angles of Eq. (11) is based on two equations (i.e. two time observations at times t and τ), if the two observed time steps are sufficiently close, the wind vector can be considered constant in the time interval $[\tau, t]$.

Under this assumption, the closed form solution of Eq. (16) becomes

$$\begin{cases} \alpha_{lin, \dot{\mathbf{w}} \approx 0} = \frac{a_{Y,t}(\dot{V}_{\infty, \tau - a_{X, \tau}}) - a_{Y, \tau}(\dot{V}_{\infty, t - a_{X, t}})}{D_{\dot{\mathbf{w}} \approx 0}} \\ \beta_{lin, \dot{\mathbf{w}} \approx 0} = \frac{a_{Z, \tau}(\dot{V}_{\infty, t - a_{X, t}}) - a_{Z, t}(\dot{V}_{\infty, \tau - a_{X, \tau}})}{D_{\dot{\mathbf{w}} \approx 0}} \end{cases}\tag{20}$$

Summarising, when the wind acceleration vector $\dot{\mathbf{w}}$ is negligible, the three existence conditions becomes

$$\begin{aligned} D_{\dot{\mathbf{w}} \approx 0} &\neq 0 \\ a_{Z_{B,t}} &\neq 0 \\ a_{Y_{B,t}} &\neq 0 \end{aligned} \quad (21)$$

5.2 Simultaneous Linearisation Accuracy

Generally speaking, according to Eq. (19) non null m_t and l_t shall be verified but more practical lower limits can be found. To this aim, two accuracy parameters are introduced in this section to evaluate the approximation error introduced with simultaneous linearisation of AoA and AoS (presented in section 3.2). A single flow angle (or independent variable) can be considered not small enough to linearise the corresponding trigonometric functions and, recalling the nonlinear system of Eq. (15), the partial linear solutions can be written as

$$\begin{aligned} \alpha_{lin}^* &= \frac{n_t - h_t (\cos \beta) - l_t (\sin \beta)}{m_t (\cos \beta)} \\ \beta_{lin}^* &= \frac{n_t - h_t (\cos \alpha) - m_t (\sin \alpha)}{l_t} \end{aligned} \quad (22)$$

Therefore, comparing Eq. (22) and Eq. (18), the proposed simultaneous linearisation of both flow angles (presented in section 3.2), introduces the following errors

$$\begin{aligned} \Delta \alpha_{lin} &= \alpha_{lin}^* - \alpha_{lin} = \frac{n_t \left(\frac{1}{\cos \beta} - 1 \right) - l_t (\tan \beta - \beta)}{m_t} \\ \Delta \beta_{lin} &= \beta_{lin}^* - \beta_{lin} = \frac{h_t (\cos \alpha - 1) + m_t (\sin \alpha - \alpha)}{l_t} \end{aligned} \quad (23)$$

As far as AoA estimation is concerned, when the β trigonometric functions are not linearised (e.g. when $\beta > 15^\circ$) and m_t tends to zero, the AoA linearisation error $\Delta \alpha_{lin} \rightarrow \pm\infty$.

As far as AoS estimation is concerned, when the α trigonometric functions are not linearised (e.g. when $\alpha > 15^\circ$) and l_t tends to zero, the AoS linearisation error $\Delta \beta_{lin} \rightarrow \pm\infty$.

In order to provide a measure of the reliability of the proposed closed form solutions of Eq. (16), two accuracy parameters are introduced as

$$\begin{aligned} K_\alpha &= \min \left(1 - \left| \frac{\Delta \alpha_{lin}}{\alpha_{lin}} \right|, 0 \right) \\ K_\beta &= \min \left(1 - \left| \frac{\Delta \beta_{lin}}{\beta_{lin}} \right|, 0 \right) \end{aligned} \quad (24)$$

where the α_{lin} and β_{lin} are those calculated with the proposed linear ASSE scheme from Eq. (16). The accuracy parameters are designed to grow up to 1 for the best estimation accuracy, whereas are null for the worst accuracy. It is worth highlighting that the accuracy parameters of Eq. (24) cannot be evaluated a priori but only after the ASSE linear estimations are performed.

In the special case when the wind acceleration is negligible (as discussed in section 5.1), the linear approximation errors of Eq. (23) can be rewritten as

$$\begin{aligned}\Delta\alpha_{lin,\dot{\mathbf{w}}\approx 0} &= \alpha_{lin,\dot{\mathbf{w}}\approx 0}^* - \alpha_{lin,\dot{\mathbf{w}}\approx 0} = \frac{1}{a_{Z_{B,t}}} \left[\dot{V}_{\infty,t} \left(\frac{1}{\cos\beta} - 1 \right) - a_{Y_{B,t}} (\tan\beta - \beta) \right] \\ \Delta\beta_{lin,\dot{\mathbf{w}}\approx 0} &= \beta_{lin,\dot{\mathbf{w}}\approx 0}^* - \beta_{lin,\dot{\mathbf{w}}\approx 0} = \frac{1}{a_{Y_{B,t}}} [a_{X_{B,t}} (\cos\alpha - 1) + a_{Z_{B,t}} (\sin\alpha - \alpha)]\end{aligned}\quad (25)$$

and the corresponding $K_{\alpha,\dot{\mathbf{w}}\approx 0}$ and $K_{\beta,\dot{\mathbf{w}}\approx 0}$ can be evaluated.

A numerical examples of the order of magnitude of $\Delta\alpha_{lin,\dot{\mathbf{w}}\approx 0}$ and $\Delta\beta_{lin,\dot{\mathbf{w}}\approx 0}$ is provided here. Typically a commercial aircraft exhibits AoA and AoS lower than 25° and body and true speed accelerations lower than 30 m s^{-2} that would lead to about unitary numerators of Eq. (25). In these circumstances, when the denominator of Eq. (25) is $\leq 1\text{ m s}^{-2}$, an error larger than 1 rad is introduced and $K_{\alpha/\beta} = 0$. This latter numerical example error is only due to the simultaneous linearisation of AoA and AoS. Therefore, recalling Eq.s (19) and (21), a practical lower limit for m_t and l_t , or $a_{Z_{B,t}}$ and $a_{Y_{B,t}}$ with negligible wind acceleration, can be set at 1 m s^{-2} otherwise they work as amplifier of the proposed simultaneous linearisation.

6. Performance of the Proposed Closed Form Solutions

In this section, the proposed scheme is verified using flight simulated data in the presence of a steady wind field. The simulation is intended to provide valid data to compare the performance of the proposed closed form solutions with the nonlinear ASSE and to discuss practical limitations of the proposed linear ASSE scheme.

6.1 Manoeuvre Definition

The flight simulated data are obtained using a coupled 6 degree of freedom nonlinear (ultralight) aircraft model equipped with nonlinear aerodynamic and thrust models designed accordingly to flight test results and the engine data sheet. The simulation is run using the explicit Euler scheme with fixed time step of 0.1 ms. The simulator does not implement any sensor noise or time delay and, hence, all signals used to solve the proposed scheme are noise-free and synchronised.

A stall manoeuvre, described in Fig. 2a, is performed to excite the angle-of-attack up to maximum values. After a short dive, the stall manoeuvre is performed producing initially an increase of airspeed and then a smooth deceleration leading to high angle-of-attack, as can be seen in Fig. 2a, with limited changes in angle-of-sideslip. The angle-of-sideslip sweep manoeuvre is performed exciting the angle-of-sideslip in a large range whereas the speed and the angle-of-attack are almost constant as can be seen in Fig. 2b.

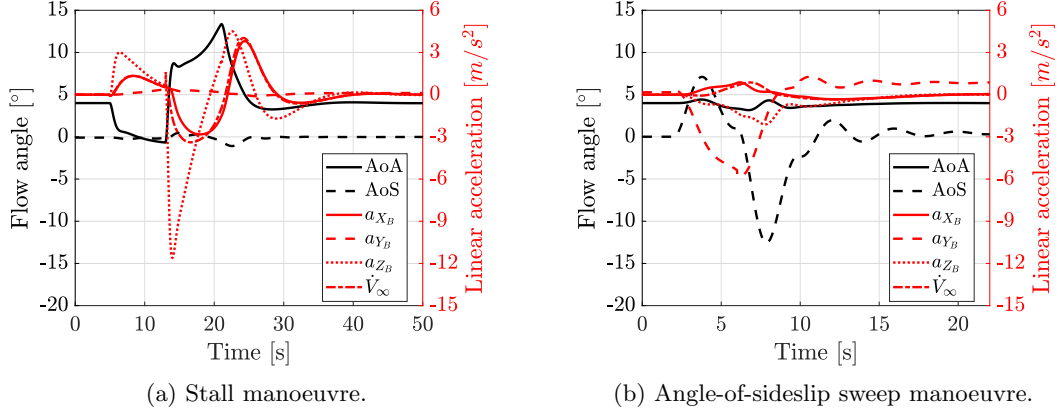


Fig. 2 Simulated flight data as in (Lerro *et al.* 2021).

From flight data reported in Fig. 2, it can be noted that, nevertheless the large variations of AoA and AoS (for the aircraft category), the linear hypothesis of Eq. (11) is still acceptable because both flow angles are $< 15^\circ$. Both manoeuvres start from trim conditions, where, as described in Section 4, the linearised ASSE scheme is not suitable.

It can be noted that in Fig. 2, excluding the trim conditions, $a_{z_B} > 1 \text{ m s}^{-2}$ for both manoeuvres, whereas $a_{y_B} < 0.5 \text{ m s}^{-2}$ during the stall manoeuvre described in Fig. 2a. According to considerations of section 5, the AoS estimation is not expected to be reliable during the stall manoeuvre.

6.2 Results

In this section the proposed linear solutions are compared with the target values (i.e. true or freestream) and results from the nonlinear ASSE scheme based on 2 equations (Lerro *et al.* 2021). AoA and AoS are estimated simultaneously using explicit solutions of Eq. (16) with the following input data: i) true airspeed; ii) true airspeed time derivative; iii) inertial body accelerations; iv) body angular rates; v) wind acceleration; vi) Euler angles (implicitly used to obtain the coordinate accelerations \mathbf{a}_B from proper accelerations commonly measured on board by inertial reference systems as described in Section 2).

The proposed linear solutions of flow angles are reported in Fig. 3 for the stall manoeuvre and in Fig. 4 for the angle-of-sideslip sweep manoeuvre. Results are summarised in Table 1 by means of the probability density function (PDF) characteristics of the estimation errors. The 1σ and 2σ values are calculated as the error of the 68.27% and 95.45% of the data points respectively.

As during the simulation the determinant is often smaller than $1 \times 10^{-6} \text{ m}^4/\text{s}^6$, the AoA and AoS estimation can be very large going beyond the aircraft physical limits. In order to avoid unrealistic estimations, evaluations beyond defined thresholds ($\pm 25^\circ$ and $\pm 35^\circ$ for AoA and AoS respectively) are discarded. This phenomena can be clearly observed at the beginning of the manoeuvre during trim conditions, for example in Fig. 3 up to 2.5 s, i.e. before the stall manoeuvre begins.

Table 1 PDF error characteristics of the flow angle estimation using the 2-equation nonlinear ASSE scheme and the proposed linearised ASSE scheme.

		2-equation nonlinear ASSE (Lerro <i>et al.</i> 2021)		Linearised ASSE	
		AoA error [°]	AoS error [°]	AoA error [°]	AoS error [°]
Stall manoeuvre	mean	0.00030	-0.0078	0.26	-2.7
	max	0.040	0.34	34	41
	1σ	0.00030	0.0017	0.26	1.8
	2σ	0.0038	0.12	1.5	22
AoS sweep manoeuvre	mean	0.0043	0.000034	0.058*	-0.058
	max	0.25	0.16	27*	39
	1σ	0.0043	0.00035	0.14*	0.10
	2σ	0.040	0.010	0.74*	0.42

*: Evaluated excluding the initial trim conditions (2 s)

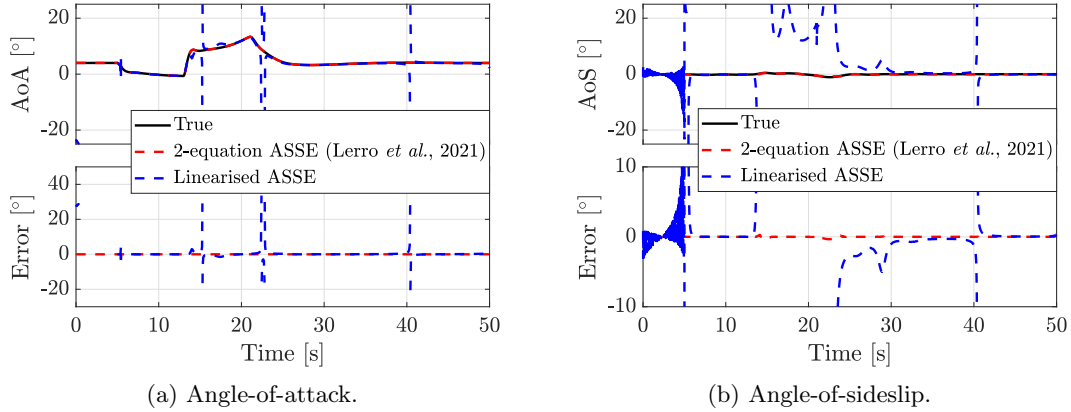


Fig. 3 Estimation using the proposed closed form solution during the simulated stall manoeuvre.

The stall manoeuvre of Fig. 3a shows very large AoA (up to 14°) whereas AoS is quite constant as a consequence of very low lateral accelerations (i.e. $a_{Y_B} < 0.5 \text{ m s}^{-2}$). The linear ASSE scheme shows a very good agreement in Fig. 3a both with true AoA and nonlinear ASSE estimation as can be observed from Table 1. In fact, the limited 2σ error (1.5°) suggests that the proposed linear AoA estimation can be reliable for the stall manoeuvre, whereas the large maximum errors (up to 34°) are only few spike errors. In the circumstance of reliable AoA linear estimation, it can be noted that the $a_{Z_B} > 10 \text{ m s}^{-2}$, whereas, the large error peaks are related to the determinant value as discussed in section 6.3.

On the contrary, the linearised ASSE scheme cannot be adopted for AoS estimation because of the very large estimation errors of Fig. 3b observed during the stall manoeuvre. In fact, along with large maximum errors (up to 41°) a large 2σ error (22°) suggests that the proposed linear AoS estimation cannot be reliable during the stall manoeuvre. Therefore,

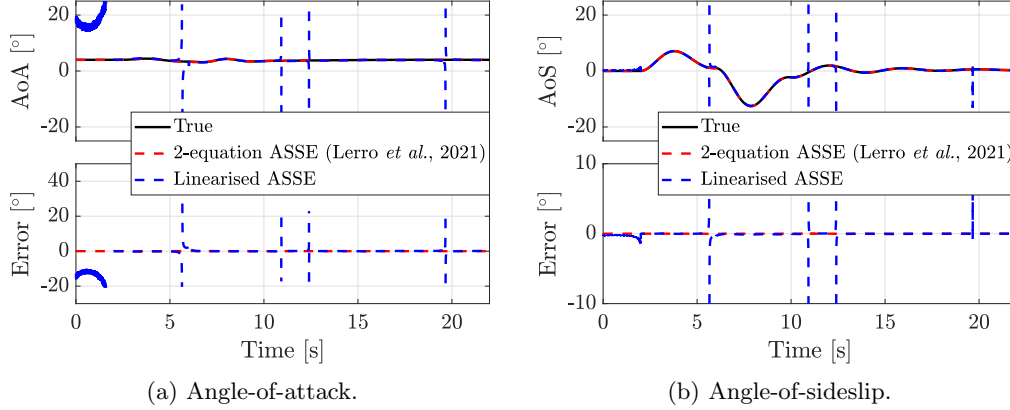


Fig. 4 Estimation using the proposed closed form solution during the simulated angle-of-sideslip sweep manoeuvre.

as introduced in section 5.2, the proposed linear scheme cannot be adopted to estimate AoS when the a_{Y_B} is smaller than 1 m s^{-2} .

From Fig. 4 it can be noted that AoS is lower than $\pm 13^\circ$ while AoA is quite constant. Excluding the initial trim conditions (up to 2s), the closed form solutions show a very good agreement for both AoA and AoS with respect to the true values and the nonlinear ASSE estimations. The limited 2σ AoS error (0.42°) suggests that the proposed linear AoS estimation can be reliable for the AoS sweep manoeuvre, whereas the large maximum errors (up to 39°) represent few spike errors. On the other side, the proposed closed form solution for AoA is reliable during the AoS sweep manoeuvre excluding the initial trim conditions as can be observed from the limited 2σ AoA error (0.74°) from Table 1. In fact, both a_{Y_B} and a_{Z_B} are $> 1 \text{ m s}^{-2}$ after the trim conditions. Moreover, the observed AoA and AoS error peaks are related to the determinant value as discussed in section 6.3.

6.3 Error Analysis

6.3.1 The Influence of the Determinant

The approximation error introduced with the zero-order ASSE approximation is detailed in (Lerro *et al.* 2021) and it was noted that is negligible, whereas the proposed linearisation introduces errors that can be very large as described in section 5. The numerical value of determinant of the proposed scheme of Eq. (15) is reported in Fig. 5 to study the relationship with the estimation error peaks of Figs. 3, 4. In particular, in Fig. 5 the determinant D is overlain on the error of the flow angle more excited in the manoeuvre (AoA for the stall manoeuvre and AoS for the sweep manoeuvre). When the estimation error is generally less than 1° , some error peaks up to $\pm 41^\circ$ can be observed.

The analysis of the stall manoeuvre of Fig. 5a clearly shows a close relationship between the value of the determinant D and the AoA error peaks. When the aircraft is manoeuvring, the AoA estimation is quite accurate except for those flight conditions that determine a very low value of D (as defined in Eq. (17)). In fact, when the determinant value drops below

$1 \times 10^{-6} \text{m}^4/\text{s}^6$, the proposed linear ASSE scheme cannot provide reliable AoA estimations.

The same conclusions can be obtained from the comparison of the AoS estimation errors and the determinant value during the angle-of-sideslip manoeuvre of Fig. 5b. Therefore, recalling Eq.s (17) and (21), the present analysis suggests that a practical lower limit for the determinant of the proposed linearised ASSE scheme is $< 1 \times 10^{-6} \text{m}^4/\text{s}^6$ in order to avoid spike errors.

6.3.2 The Influence of the Accuracy Parameters

In Fig. 6 the estimation error of the proposed closed form solutions is overlain to the corresponding accuracy parameters introduced in section 5. The plots are only referred to the flow angle that showed larger errors (AoS for the stall manoeuvre and AoA for the sweep manoeuvre).

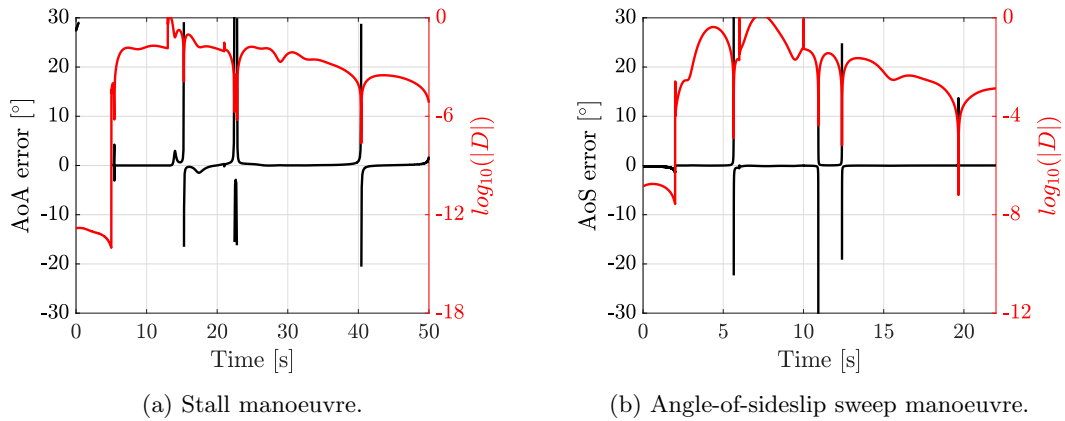


Fig. 5 Determinant value of the linearised ASSE scheme compared with AoA and AoS estimation errors.

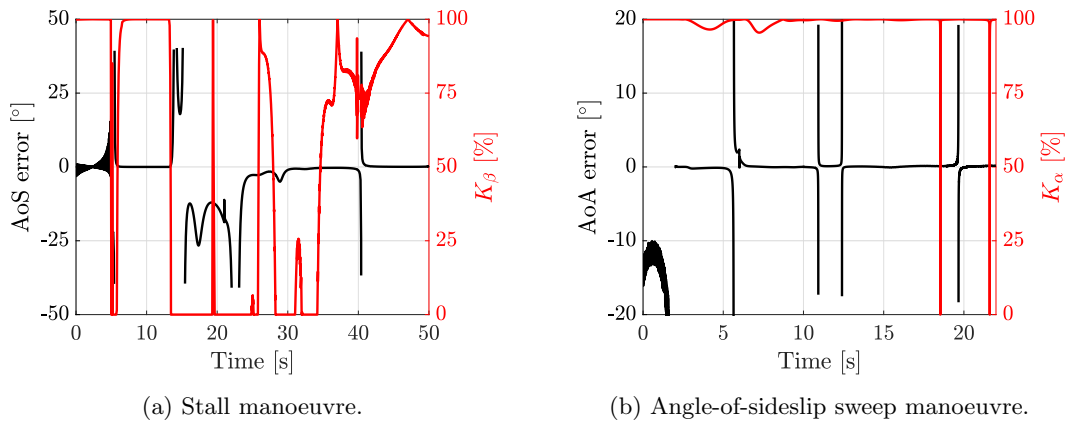


Fig. 6 Accuracy parameter value compared with AoS and AoA estimation error respectively.

It can be observed in Fig. 6b that K_α is generally $> 90\%$ during the angle-of-sideslip sweep manoeuvre and, therefore, the approximation error introduced with the linear ASSE scheme is negligible for AoA estimation.

On the contrary, for the stall manoeuvre of Fig. 6a, K_β is generally $< 50\%$ and, in fact, the corresponding AoS linear estimation shows large errors ($> 5^\circ$). Nevertheless, it can be noted that when $K_\beta > 75\%$ a reliable linear AoS estimation is provided in the corresponding time intervals. Therefore, based on results presented in this section, the proposed lower limit of the accuracy parameters is 75% .

6.3.3 Error Analysis Implications

From results of section 6.2 and the error analysis of sections 6.3.1 and 6.3.2, three parameters can be evaluated to recognise when the proposed closed form solutions can be used to replace the nonlinear ASSE scheme for AoA and AoS estimations:

1. determinant of Eq. (16): $D > 1 \times 10^{-6} \text{m}^4/\text{s}^6$
2. vertical / lateral proper acceleration:
 - $a_{Z_B} > 1 \text{ m s}^{-2}$ for estimation of AoA
 - $a_{Y_B} > 1 \text{ m s}^{-2}$ for estimation of AoS
3. proposed accuracy parameter:
 - $K_\alpha > 75\%$ for estimation of AoA
 - $K_\beta > 75\%$ for estimation of AoS

Therefore, according to the specific flow angle estimation, only when all of the three above conditions are verified, the proposed closed form solution can be adopted rather than solving the nonlinear ASSE scheme.

7. Conclusion

A physics-based modelling is introduced to estimate flow angles, angle-of-attack and angle-of-sideslip, using a nonlinear scheme. The linearisation of the nonlinear scheme leads to a system of two linear equations whose solutions are explicitly written. The proposed closed form solutions for angle-of-attack and angle-of-sideslip are based on the direct measure of true airspeed, angular rates, inertial accelerations, aircraft attitudes and wind acceleration vector. As far as the linear algebra existence conditions are concerned, it is demonstrated that the proposed closed form solution is only applicable during dynamic conditions, e.g. when the system determinant is nonzero. Moreover, simultaneous linearisation of flow angles can introduce large errors that can be identified using the two accuracy parameters proposed with this work. It is clear that the closed form solutions are more straightforward if compared to the nonlinear scheme but, considering the numerical verification using flight simulated data, it emerged that AoA and AoS linear solution accuracy can be compromised due to several recognisable limitations. From result analysis, three limitations are introduced to recognise

in real-time applications when the linearised solutions are as reliable as the nonlinear scheme. Therefore, the proposed closed form solutions for flow angle estimation can only be adopted as a partial replacement of the nonlinear ASSE scheme.

References

- Colgren, R., Frye, M. and Olson, W. (1999), “A proposed system architecture for estimation of angle-of-attack and sideslip angle”, in “Guidance, Navigation, and Control Conference and Exhibit”, c, pages 743–750, American Institute of Aeronautics and Astronautics, Reston, Virginia, URL <http://arc.aiaa.org/doi/10.2514/6.1999-4078>.
- Dendy, J. and Transier, K. (1969), *Angle-of-Attack Computation Study*, Technical report, Air Force Flight Dynamics Laboratory, aFFDL-TR-69-93.
- Etkin, B. and Reid, L. (1995), *Dynamics of Flight: Stability and Control; Third Edition*, Wiley.
- Eubank, R., Atkins, E. and Ogura, S. (2010), “Fault Detection and Fail-Safe Operation with a Multiple-Redundancy Air-Data System”, in “AIAA Guidance, Navigation, and Control Conference”, August 2010, pages 1–14, American Institute of Aeronautics and Astronautics, Reston, Virginia, URL <http://arc.aiaa.org/doi/10.2514/6.2010-7855>.
- Fravolini, M.L., Del Core, G., Papa, U., Valigi, P. and Napolitano, M.R. (2019), “Data-Driven Schemes for Robust Fault Detection of Air Data System Sensors”, *IEEE Transactions on Control Systems Technology*, **27**(1), 234–248.
- Freeman, D.B. (1973), *Angle of Attack Computation System*, Technical report, Air Force Flight Dynamics Laboratory, aFFDL-TR-73-89.
- Gavrilovic, N., Bronz, M., Moschetta, J.M. and Benard, E. (2018), “Bioinspired wind field estimation—part 1: Angle of attack measurements through surface pressure distribution”, *International Journal of Micro Air Vehicles*, **10**(3), 273–284, URL <https://doi.org/10.1177/1756829318794172>, <https://doi.org/10.1177/1756829318794172>.
- Lerro, A., Brandl, A. and Gili, P. (2021), “Model-Free Scheme for Angle-of-Attack and Angle-of-Sideslip Estimation”, *Journal of Guidance, Control, and Dynamics*, **44**(3), 595–600.
- Lu, P., van Kampen, E.J., de Visser, C. and Chu, Q. (2020), “Air Data Sensor Fault Detection and Diagnosis in the Presence of Atmospheric Turbulence: Theory and Experimental Validation With Real Flight Data”, *IEEE Transactions on Control Systems Technology*, pages 1–9.
- Marzat, J., Piet-Lahanier, H., Damongeot, F. and Walter, E. (2012), “Model-based fault diagnosis for aerospace systems: a survey”, *Proceedings of the Institution of Mechanical Engineers, Part G: Journal of Aerospace Engineering*, **226**(10), 1329–1360, URL <https://doi.org/10.1177/0954410011421717>, <https://doi.org/10.1177/0954410011421717>.
- Nelson, R. (1989), *Flight stability and automatic control*, McGraw-Hill series in aeronautical and aerospace engineering, McGraw-Hill Ryerson, Limited.
- Popowski, S. and Dabrowski, W. (2015), “Measurement and estimation of the angle of attack and the angle of sideslip”, *Aviation*, **19**(1), 19–24.
- Pouliezios, A.D. and Stavrakakis, G.S. (1994), “Analytical Redundancy Methods”, in “Real Time Fault Monitoring of Industrial Processes”, volume 12, pages 93–178, Springer Netherlands, Dordrecht, URL https://doi.org/10.1007/978-94-015-8300-8_2.
- Salychev, O.S. (2004), *Applied Inertial Navigation: Problems and Solutions*, BMSTU Press.
- Schmidt, D. (2011), *Modern Flight Dynamics*, ASIA HIGHER EDUCATION ENGINEER, McGraw-Hill, URL <https://books.google.it/books?id=TofEXwAACAAJ>.

- Sun, K., Regan, C.D. and Egziabher, D.G. (2018), “GNSS/INS based estimation of air data and wind vector using flight maneuvers”, in “2018 IEEE/ION Position, Location and Navigation Symposium (PLANS)”, pages 838–849, IEEE, URL <https://ieeexplore.ieee.org/document/8373461/>.
- Tian, P., Chao, H., Rhudy, M., Gross, J. and Wu, H. (2021), “Wind Sensing and Estimation Using Small Fixed-Wing Unmanned Aerial Vehicles: A Survey”, *Journal of Aerospace Information Systems*, **18**(3), 132–143, URL <https://doi.org/10.2514/1.I010885>, <https://doi.org/10.2514/1.I010885>.

EC